Xenobiotica, March 2005; 35(3): 253–271

Taylor & Francis
Taylor & Francis Group

Pre-clinical assessment of DRF 4367, a novel COX-2 inhibitor: Evaluation of pharmacokinetics, absolute oral bioavailability and metabolism in mice and comparative inter-species *in vitro* metabolism

R. BHAMIDIPATI[1], S. MUJEEB[1], P. V. DRAVID[1], A. A. KHAN[1], S. K. SINGH[2], Y. K. RAO[2], R. MULLANGI[1], & N. R. SRINIVAS[1]

[1]*Drug Metabolism and Pharmacokinetics, Discovery Research, Dr. Reddy's Laboratories Ltd, Miyapur, Hyderabad, India, and* [2]*Discovery Chemistry, Discovery Research, Dr. Reddy's Laboratories Ltd, Miyapur, Hyderabad, India*

(Received 1 November 2004)

Abstract

The aim of this study was to characterize the pharmacokinetics and determine the absolute bioavailability and metabolism of DRF 4367, a novel COX-2 inhibitor, in mice. In addition, the *in vitro* metabolism of DRF 4367 was studied in mouse, rat, dog, monkey and human liver microsomes. Following oral administration, maximum concentrations of DRF 4367 were achieved after about 1 h. Upon intravenous (IV) administration, the concentration of DRF 4367 declined in a bi-exponential fashion with a terminal elimination half-life of 4.0 h. The elimination half-life was unchanged with route of administration. The volume of distribution and systemic clearance of DRF 4367 in mice were 0.80 $l h^{-1} kg^{-1}$ and 0.14 $l kg^{-1}$, respectively, after IV administration. The absolute oral bioavailability of DRF 4367 was 44%. In all species of liver microsomes examined, the primary route of metabolism for DRF 4367 was demethylation of benzyl methoxy to form a hydroxy metabolite (M1). The formation of this metabolite was mediated by CYP2D6 and CYP2C19 enzymes. M1 was not found to possess COX-2 inhibitory activity. Chemical-inhibition studies showed that quinidine (selective for CYP2D6) and ticlopidine (selective for CYP2C19) inhibited the formation of the hydroxy metabolite of DRF 4367, whereas potent inhibitors selective for other forms of CYP did not inhibit this oxidative reaction. Upon oral or IV administration of DRF 4367 to mice, unchanged DRF 4367, M1, the *O*-glucuronide conjugate of M1 (M1-G) and the *O*-sulfate conjugate of M1 (M1-S) were identified in bile.

Keywords: *DRF 4367, mice, pharmacokinetics, bioavailability, metabolism*

Correspondence: N. R. Srinivas, Drug Metabolism and Pharmacokinetics, Discovery Research, Dr. Reddy's Laboratories Ltd, Miyapur, Hyderabad-500 049, India. Fax: +91-40-23045438. E-mail: nrsrinivas@drreddys.com

ISSN 0049-8254 print/ISSN 1366-5928 online
DOI: 10.1080/00498250500066303

Introduction

Cyclooxygenase (COX), an enzyme that catalyzes the conversion of arachidonic acid into prostaglandin (PG) and thromboxane, was considered for a long time to be responsible for both the therapeutic and adverse effects of non-steroidal anti-inflammatroy drugs (NSAIDs) (Graul et al. 1997; Riendeau et al. 1997; Vane et al. 1998). COX-1 is the major form located in tissues, and it plays a role in thrombogenesis and homeostastis of the gastrointestinal tract and kidney (Smith and DeWitt 1996). In contrast, COX-2 is normally undetectable in most tissues and is inducible by cytokines, endotoxins and mitogens. Current NSAIDs inhibit both forms of the enzyme, and it is believed that it is the inhibition of COX-1 that causes the side effects seen with NSAIDs. The discovery of COX-2 led to the recognition that selective inhibitors of COX-2 constitute a novel approach in the treatment of inflammation with diminished side effects. The hypothesis was proven when the first selective compounds, NS-398 and DuP-697, were tested (Gierse et al. 1995). After this discovery, several laboratories extensively worked on selective COX-2 inhibitors (coxibs). Recently, a few diarylheterocycle coxibs, namely celecoxib, rofecoxib, valdecoxib and etoricoxib, were shown to possess anti-inflammatory activity with little or no gastric side effects (DeWitt 1999). In the course of our program aiming to discover new COX-2 molecules, our efforts in synthesis and systematic structure–activity relationship studies identified DRF 4367 as a novel, potent COX-2 inhibitor. DRF 4367 (Figure 1) is 2-hydroxymethyl-4-[5-(4-methoxyphenyl)-3-trifluoromethyl-1H-1-pyrazolyl]-1-benzene sulfonamide. It exhibits potent COX-2 selectivity in *in vitro* studies and dose-proportional pharmacokinetics in Wistar rats (Ramesh et al. 2003; Singh et al. 2004). As part of the preclinical profiling of DRF 4367, the present investigation was undertaken to characterize the oral bioavailability, pharmacokinetics and metabolism of DRF 4367 in mice and comparative interspecies *in vitro* metabolism.

Materials and methods

Chemicals and reagents

DRF 4367, DRF 6574 (Figure 1) and celecoxib (I.S, Figure 1) were synthesized by the Medicinal Chemistry Group, Discovery Research, Dr. Reddy's Laboratories Ltd (DRL), Hyderabad, India and were characterized using chromatographic and spectral techniques by Analytical Research Group, DRL. The purity was found to be more than 99% for all of these compounds. Acetonitrile, methanol, dichloromethane, formic acid and ethyl acetate were of HPLC grade (Qualigens, Mumbai, India), and potassium dihydrogen orthophosphate, hydrochloric acid, ethylene diamine tetra-acetic acid disodium salt (EDTA) and phosphoric acid and magnesium chloride were of Analytical Reagent grade (Qualigens, Mumbai, India). Cremophor ELP, dimethyl sulfoxide (DMSO), mercapto-ethanol, $NADP^+$, quinidine, sodium carboxy methyl cellulose, ticlopidine hydrochloride, trizma base, 3′-phosphoadenosine-5′-phosphosulfate (PAPS), UDP-glucuronic acid (UDPGA) were obtained from Sigma-Aldrich (Milwaukee, WI). All other reagents used were of Laboratory Reagent grade and were used without further purification. All aqueous solutions including buffer for HPLC and LC-MS/MS mobile phase were prepared in Milli Q (Millipore, Milford, MA)-grade water. Pooled liver microsomes of male Wistar rats, male Beagle dogs, male Cynomolgus monkeys and male humans were obtained from In-Vitro Technologies (Baltimore, MD), whereas male Swiss Albino mice liver microsomes were prepared in-house, and CYP enzymes (Bactosomes) were procured from Cypex Ltd (Dundee, UK).

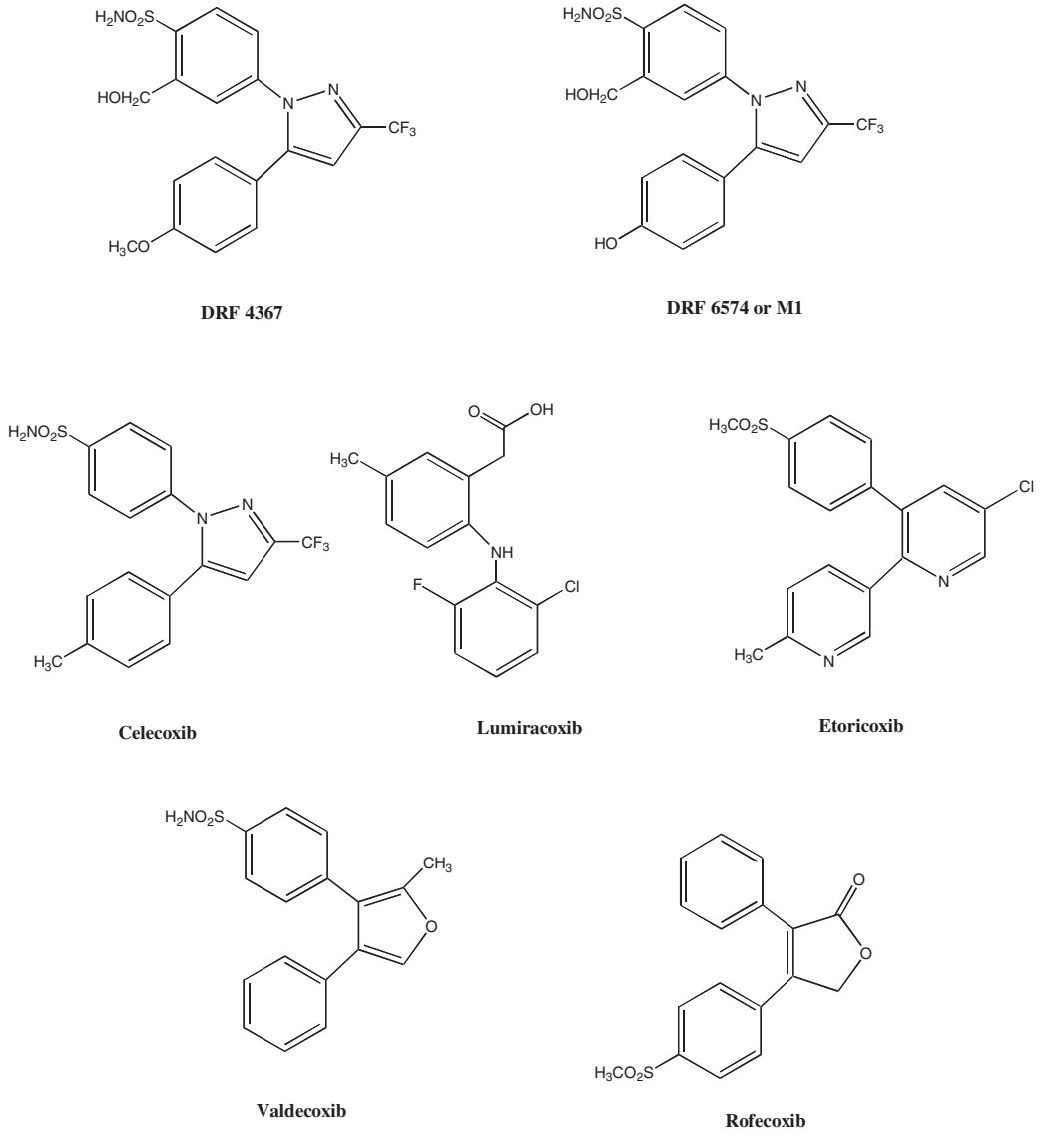

Figure 1. Chemical structures of DRF 4367, DRF 6574 or M1, celecoxib, etoricoxib and valdecoxib.

Animals

Male Swiss Albino mice (bred in DRL animal facility), 6–8 weeks of age and weighing 24–32 g, were used in the present study. All animal experiments were approved by the DRL Institutional Animal Ethics Committee and were in accordance with the Committee for the Purpose of Control and Supervision of Experiments on Animals (CPCSEA), Ministry of Social Justice and Environment, Government of India. Animals were maintained on normal laboratory chow (National Institute of Nutrition, Hyderabad, India), with water ad libitum, and a 12 h light/dark cycle. For all the studies, the animals were deprived of food 14 h before dosing but had free access to water.

Pharmacokinetic studies and animal experiments

Pharmacokinetic and absolute oral bioavailability assessment of DRF 4367 were evaluated in a parallel-group study in male Swiss Albino mice. DRF 4367 was administered by oral gavage at a dose of 10 mg kg^{-1}, as a suspension in 0.25% sodium carboxymethylcellulose to a group of mice ($n = 12$). In another experiment, a solution of DRF 4367 in 20% hydroxypropyl-β-cyclodextrin containing 3% DMSO was administered to mice ($n = 10$) via the tail vein as a bolus dose of 10 mg kg^{-1}. Animals were provided with standard diet 3 h after dosing. Blood samples (~0.25 ml, sparse sampling procedure) were collected from the retro-orbital plexus at 0.17 (only for IV), 0.25, 0.5, 1, 2, 4, 6, 8, 10 and 24 h time points into micro-centrifuge tubes containing 10 µl of saturated solution of EDTA. Plasma was harvested by centrifuging the blood using Biofuge (Hereaus, Germany) at 7500*g* for 5 min. Plasma was transferred into polypropylene tubes and stored frozen at −80°C till bioanalysis. Bile was collected from three mice hourly for 8 h directly into microcentrifuge tubes containing 100 µl of 0.1 M ammonium acetate buffer, pH 4.5. Bile was subjected to mass spectral analysis before and after treatment with 500 units ml^{-1} of β-glucuronidase (free of arylsulfatase) or arylsulfatase (Remmel et al. 2004). Urine and feces were collected continuously from three mice over a period of 24 h. All the samples were frozen and kept immediately at −20°C.

In vitro *metabolism studies*

Phase I enzyme assay. The incubation mixtures of DRF 4367 with liver microsomes (mice, rat, dog, monkey and human) contained the following at the indicated final concentrations (final volume of 500 µl): 100 mM potassium phosphate buffer (pH 7.4), microsomes (1 mg ml^{-1}), 1 mM $NADP^+$, glucose-6-phosphate (10 mM), glucose-6-phosphate dehydrogenase (2 units ml^{-1}), and $MgCl_2$ (5 mM). The mixtures were pre-incubated at 37°C for 5 min. The metabolism reaction (in triplicate) was initiated by addition of DRF 4367 (10 µM, added as methanolic solution with a final methanol concentration of 1%). After 30 min incubation, the reaction was terminated by addition of 400 µl of ethyl acetate and vortexed. The mixtures were extracted, processed and analyzed by HPLC and LC-MS/MS as described below.

Thermal inactivation of flavin-containing monooxygenases (FMOs) in microsomes was performed by pre-incubation of the above mixture without NADPH for 10 min at 37°C. In parallel, controls were pre-incubated in the presence of NADPH (which protects the enzymes from denaturation). DRF 4367 and NADPH were then added to both samples before the incubation. Methimazole oxidase activity was checked to confirm inactivation of FMO at 37°C as previously described (Teyssier and Siess 2000). The non-selective CYP inhibitor, 1-aminobenzotriazole (ABT), was used to assess overall contribution of CYP metabolism. 1-ABT dissolved in methanol was used, and the concentration of methanol in the incubation medium was less than 0.5%.

Appropriate P450 inhibitors (CYP1A2-furaphylline; CYP2A6-diethyldithiocarbamate; CYP2C9-diazepam; CYP2C19-ticlopidine; CYP2D6-quinidine; CYP2E1-disulfiram and CYP3A4-ketoconazole and troleandomycin) were added to the incubation mixture, which contained non-induced microsomes to assess the enzymes involved (Teyssier and Siess 2000). The inhibitors were dissolved in ethanol, and the concentration of ethanol in the incubation medium was less than 0.1%.

Identification of CYP enzymes involved in phase I metabolism

To identify the CYP enzymes responsible for metabolism of DRF 4367, incubations were conducted as described above, except that baculovirus-expressed P450 enzymes (CYP1A1, CYP1A2, CYP2A6, CYP2B6, CYP2C8, CYP2C9, CYP2C19, CYP2D6, CYP2E1 and CYP3A4) were used at a concentration of 50 pmol ml^{-1} for the incubation. DRF 4367 was used at a final concentration of 10 μM in these experiments. Positive controls were run concurrently to ensure microsomal viability and included: de-ethylation of 7-ethoxyresorufin (CYP1A1), de-ethylation of 3-cyano-7-ethoxycoumarin (CYP1A2 and CYP2C19), hydroxylation of coumarin (CYP2A6), de-ethylation of 7-ethoxy trifluoromethyl coumarin (CYP2C8), dealkylation of dibenzylfluorescein (CYP2C9), de-ethylation of 3-[2-(*N*,*N*-diethyl-*N*-methyl-amino) ethyl]-7-methoxy-4-methylcoumarin (CYP2D6), hydroxylation of *p*-nitrophenol (CYP2E1) and the dealkylation of resorufin benzyl ether (CYP3A4).

Phase II enzyme assays. Glucuronidation was investigated by incubating microsomal proteins (mice, rat, dog, monkey and human; 0.5 mg ml^{-1}) at 37°C for 60 min in a medium (0.5 ml) containing 40 mM Tris buffer (pH 7.4), 5 mM $MgCl_2$, 2 mM uridine diphospho-α-D-glucuronic acid (UDPGA), and 10 μM DRF 4367 or DRF 6574. After incubation for 60 min, the reaction was terminated by addition of 1 N HCl (Gradolatto et al. 2004). The mixtures were mixed and centrifuged (for 10 min at 2000*g*), and the clear supernatant was analyzed by HPLC and LC-MS/MS as described below.

Sulfation was investigated by incubating cytosolic proteins (mice, rat, dog, monkey and human; 1 mg ml^{-1}) at 37°C for 60 min in a medium (0.5 ml) containing 40 mM Tris buffer (pH 7.4), 5 mM $MgCl_2$, 3 mM mercaptoethanol, 0.2 mM 3′-phosphoadenosine-5′-phosphosulfate (PAPS) and 10 μM DRF 4367 or DRF 6574. After incubation for 60 min, the reaction was terminated by addition of 500 μl of cold methanol and vortexing (Gradolatto et al. 2004). The mixtures were mixed and centrifuged (for 10 min at 2000*g*), and the clear supernatant was analyzed by HPLC and LC-MS/MS as described below.

The mixed reaction of conjugation (sulfation and glucuronidation) was investigated by incubating mice, rat, dog, monkey and human microsomal and cytosolic proteins (0.5 and 1 mg ml^{-1}, respectively) at 37°C for 3 h in a medium containing 50 mM Tris buffer (pH 7.4), 5 mM $MgCl_2$, 3 mM mercaptoethanol, 2 mM UDPGA, 0.2 mM PAPS and 1 mM substrate. The reaction was stopped by adding 500 μl of cold methanol and vortexing. The mixtures were mixed and centrifuged (for 10 min at 2000*g*), and the clear supernatant was analyzed by HPLC and LC-MS/MS as described below.

Sample preparation and analysis

Two different reverse-phase HPLC methods were used for measuring DRF 4367 in pharmacokinetic studies and unchanged DRF 4367, and its metabolites formed *in vitro* after incubation in liver microsomes and c-DNA expressed CYPs. The metabolites formed during phase I, phase II and *in vivo* metabolism were identified by liquid chromatography-mass spectrometry.

Method 1 (HPLC analysis of plasma samples). Plasma samples were processed and analyzed using a validated high-performance liquid chromatography (HPLC) with UV detection method (Ramesh et al. 2004). Briefly, to an aliquot of 100 μl of plasma sample, methanolic solution of celecoxib (internal standard) equivalent to 1 μg was added and mixed on a cyclomixer (Remi Instruments, Mumbai, India). After the addition of 3 ml of

dichloromethane, the mixture was vortexed for 2 min, followed by centrifugation for 10 min at 1760*g* on a tabletop centrifuge (Remi Instruments, Mumbai). The clear organic layer (2.7 ml) was separated and evaporated to dryness at 40°C using a gentle stream of nitrogen (Zymark® Turbovap®, Kopkinton, MA). The residue was reconstituted in 150 µl of the mobile phase, and 50 µl was injected onto the HPLC column. Chromatography was carried out using a Shimadzu Class-VP series module (Kyoto, Japan). The isocratic mobile phase consisting of 0.01 M potassium dihydrogen orthophosphate buffer, pH 3.2 and acetonitrile mixture (40:60, v/v) was run at a flow rate of 1 ml min^{-1}. Chromatographic separation was achieved using Kromasil KR100-5C18-250A, 5 µm, 4.6 × 250 mm column (Hichrom, Theale, UK). The eluate was monitored by an UV detector set at 247 nm. The retention times of DRF 4367 and the internal standard were 6.6 and 11.0 min, respectively.

Method 2 (HPLC analysis of DRF 4367 and phase I metabolites in incubations using liver microsomes and c-DNA expressed CYPs). Samples from metabolism studies were analyzed for DRF 4367 and the appearance of potential metabolites by a modified HPLC method reported earlier (Rao et al. 2003). Briefly, the samples were extracted with ethyl acetate, and the organic layer was evaporated to dryness at 40°C using a gentle stream of nitrogen and reconstituted in 150 µl of mobile phase, and 50 µl was injected onto HPLC column. Chromatography was carried out using a Waters 2695 Alliance (Milford, MA) separation module attached with a Waters® 2996 photodiode array (PDA) detector. An Inertsil® ODS 3V column (4.6 × 250 mm, 5 µm, GL Sciences Inc., Tokyo) was used for the analysis. The ternary mobile phase system consisting of reservoir-A (0.05 M formic acid, pH 3.2), reservoir-B (Milli Q water:acetonitrile; 10:90) and reservoir-C (Milli Q water:methanol; 10:90) was run as per the gradient program (Rao et al. 2003) with a total flow rate of 1.0 ml min^{-1} throughout the analysis. Eluate was monitored through PDA detector (scan range: 200–400 nm), and data integration was carried out using Millennium^{32} software (version 4).

Mass spectrometry analysis (verifying metabolites formed in incubations using c-DNA expressed CYPs and phase II metabolism studies). Analyses of the metabolites were performed under the HPLC conditions described in method 2. An interface was established between an Agilent (Agilent Technologies, Waldbronn, Germany) 1100 series LC system equipped with degasser (G1322A), isopump (G1310A) and colcom (G1316A), Gilson 215 Model liquid handler (Gilson Inc., Middleton, WI) and a PE Sciex (Foster City, CA) API 3000 triple quadruple mass spectrometer, equipped with a Turboionspray™. Samples were either injected (50 µl volume) onto a 5-µm Inerstil® ODS-3V column (4.6 × 250 mm, GL Science Inc., Tokyo) kept at ambient temperature or infused with a peristaltic pump (at a rate of 5 µl min^{-1}) into the mass spectrometer. Mass spectra were acquired in selective ion-recording mode or full scans from $m/z = 200$ to 800 at 1/scan/s. Both positive and negative ion monitoring with scanning mode were performed at a capillary voltage of 3500 V. The operating conditions were as follows: ionization voltage, 5 kV; nitrogen curtain gas setting, 15; collision energy, ~45 eV; declustering and focusing potentials, 80 and 260 V, respectively. CID studies were performed using collision energy of 45 eV and a collision cell of argon gas with the pressure at 2×10^{-3} mbar. Authentic standards of DRF 4367 [$(M+H)^+$ ion at m/z 427] and its phase I metabolite [DRF 6574, $(M+H)^+$ ion at m/z 413] were available to support the standard chromatographic retention time, UV spectra and MS results in structural assignment.

Pharmacokinetic data analysis

Pharmacokinetic parameters were calculated using a non-compartmental method (Gibaldi and Perrier 1982). The peak plasma concentration (C_{max}) and the corresponding time (T_{max}) were directly obtained from the raw data. The area under the plasma concentration versus the time curve up to the last quantifiable time point, $AUC_{(0-t)}$ was obtained by the linear and log-linear trapezoidal summation. The $AUC_{(0-t)}$ extrapolated to infinity (i.e. $AUC_{(0-\infty)}$) by adding the quotient of C_{last}/K_{el}, where C_{last} represents the last measurable time concentration, and K_{el} represents the apparent terminal rate constant. K_{el} was calculated by the linear regression of the log-transformed concentrations of the drug in the terminal phase. The half-life of the terminal elimination phase was obtained using the relationship $t_{1/2} = 0.693/K_{el}$. The concentration at zero time, C_0, following IV administration was calculated by extrapolating the logarithmic plasma concentration versus the time plot of the IV plasma concentration profile to zero time (y-axis). Systemic clearance was calculated by the relationship $CL = (D_{IV})/AUC_{(0-\infty)IV}$ where D_{IV} is the dose of the compound. The apparent volume of distribution was obtained from the equation $V_d = D/(AUC_{(0-\infty)} \times K_{el})$. The absolute oral bioavailability (F) was calculated using the relationship, $F = [\text{dose (IV)} \times AUC_{(0-\infty)oral}/\text{dose (oral)} \times AUC_{(0-\infty)IV}] \times 100$.

Results

Pharmacokinetic studies

The plasma concentration–time profiles of DRF 4367 after IV and oral administration are shown in Figure 2, and a summary of the pharmacokinetic parameters is shown in Table I. Following IV administration of DRF 4367 to mice, the plasma concentrations declined in a bi-exponential fashion with a terminal half-life of 3.99 h. Systemic exposure, volume of distribution and clearance of DRF 4367 were 71.79 $\mu g\,h\,ml^{-1}$, 0.80 $l\,h^{-1}\,kg^{-1}$ and 0.14 $l\,kg^{-1}$, respectively. After oral administration, DRF 4367 reached maximum plasma levels within 1.0 h. DRF 4367 could be detected in mouse plasma 24 h after oral or IV dosing (Figure 2). The elimination following oral administration was found to be comparable to the IV route (Table I). The absolute oral bioavailability of DRF 4367 at 10 $mg\,kg^{-1}$ was found to be 44%. Regardless of the route of administration, we observed a plateauing effect in the concentration vs time profile at 6–10 h post-dose, which may be attributable to the presence of the entero-hepatic recirculation phenomenon.

Metabolism by phase I enzymes

A comparison of the metabolic stability (disappearance rate) of DRF 4367 in liver microsomes of various animal species, namely mouse, rat, dog, monkey and human, is presented in Figure 3. The percentage dose of DRF 4367 metabolized in 30 min was 20.7, 21.3, 10.0, 40.1 and 28.5 in mouse, rat, dog, monkey and human, respectively. *In vitro* metabolism experiments carried out with liver microsomes supplemented with NADPH and subsequent HPLC analysis of incubation mixture extracts revealed the formation of one metabolite (M1 or DRF 6574), which eluted at 31.2 min and appeared to be linear with respect to incubation time in liver microsomes of various animal species tested. A typical HPLC chromatogram depicting DRF 4367 metabolism in mouse liver microsomes in the presence of NADPH is shown in Figure 4. LC-MS analysis of M1, which was formed with all liver microsomes of various animal species indicated a deprotonated molecular ion $(M - H)^+$ at m/z 412, suggesting demethylation of the parent

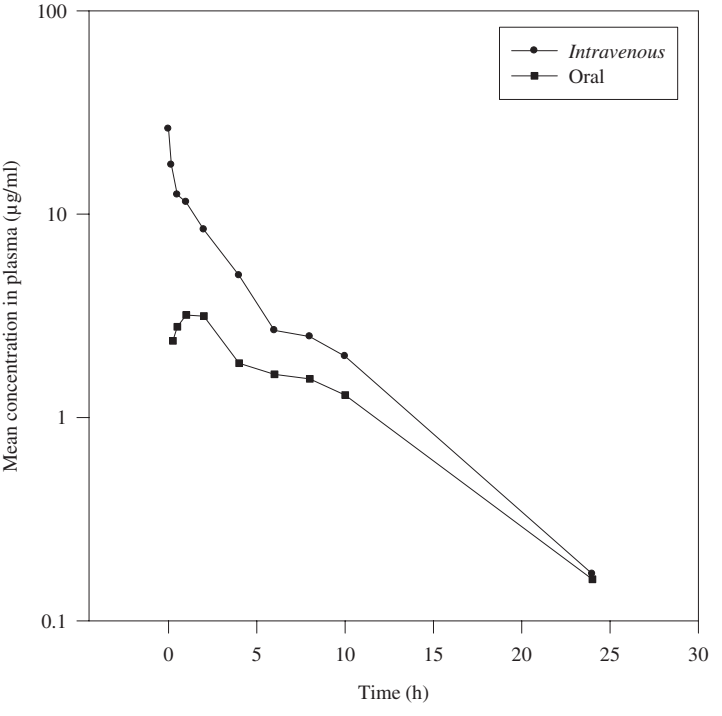

Figure 2. Mean plasma concentration–time curves of DRF 4367 in mice following oral and *intravenous* administration at 10 mg kg^{-1}. Data are derived from of 12 animals.

Table I. Pharmacokinetic parameters for DRF 4367 in mice after oral and intravenous administration to mice at 10 mg kg^{-1}[a].

Pharmacokinetic parameters	Oral	Intravenous
$AUC_{(0-\infty)}$ (μg h ml^{-1})	31.4	71.79
C_{max} (μg ml^{-1})	3.19	26.25
T_{max} (h)	1.00	–
K_{el} (h^{-1})	0.140	0.174
$t_{1/2}$ (h)	4.80	3.99
Cl (l h^{-1} kg^{-1})	–	0.14
V_d (l kg^{-1})	–	0.80
F (%)	44	–

[a]Data are derived from the mean of 12 animals.

compound. Further, the structure of the metabolite was confirmed by comparison of chromatographic and MS data with the synthetic standard material, i.e. DRF 6574. The CID spectrum of *m/z* 412 generated a series of product ions at *m/z* 382, 364, 331, 328, 318, 303 and 80 (Figure 5), which matched the mass spectrum of the authentic synthetic standard (DRF 6574). The sequential loss of 30 (CH_2OH), 18 (F) and 36 (2 F) Da from *m/z* 412 generated the product ions at *m/z* 382, 364 and 328, respectively. The product ion at *m/z* 331 was generated directly from *m/z* 412 due to 81 (O_2NH_2, OH and F) Da. The sequential loss of 64 (SO_2) and 15 (NH_2) Da from *m/z* 382 generated the product ions

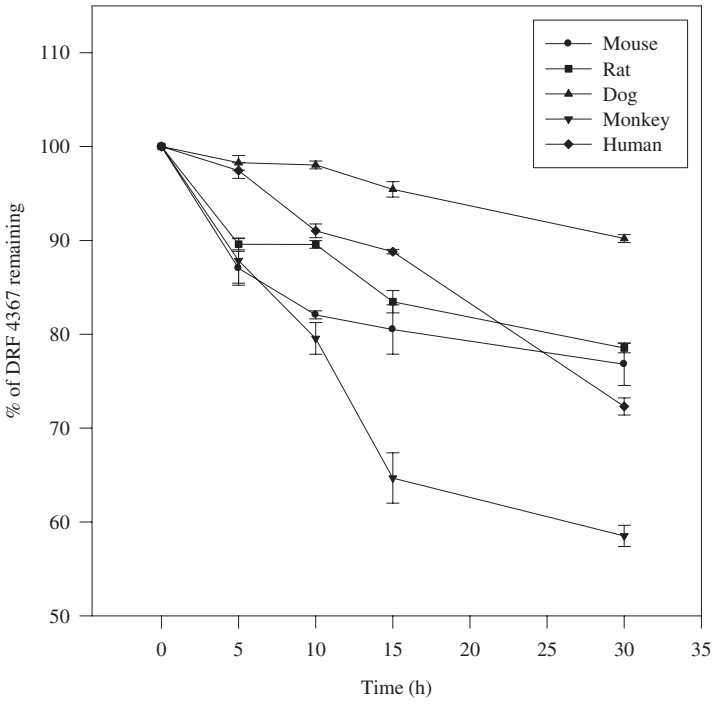

Figure 3. Disappearance of DRF 4367 in incubation from mouse, rat, dog, monkey, and human liver microsomes. Data are derived from three determinations.

at *m*/*z* 318 and 303, respectively. The product ion at *m*/*z* 80 corresponds to the SO_2NH_2 group. Based on these data, M1 was identified as demethylated metabolite of DRF 4367. The parent compound, which eluted at 32.3 min, showed a similar CID spectrum to the authentic synthetic standard. The CID spectrum of *m*/*z* 426 generated a series of product ions at *m*/*z* 396, 364, 332, 317, 303, 80 and 69 (Figure 6). The sequential loss of 30 (CH_2OH), 32 (O_2), 32 (S), 15 (NH_2) and 14 (CH_3) Da from *m*/*z* 426 generated the product ions at *m*/*z* 396, 364, 332, 317 and 303. The product ions at *m*/*z* 80 and 69 correspond to SO_2NH_2 and CF_3 groups, respectively.

As the metabolism of DRF 4367 occurred only in the presence of NADPH, CYPs and/or FMO are probably involved. No change in the metabolism of DRF 4367 was observed following thermal inactivation of FMO (data not shown). When the reaction took place in the presence of 1-ABT (non-specific CYP inhibitor), the formation of M1 was reduced by ~95% (data not shown). Thus, these results suggest that CYPs are the main mediators of phase I enzyme reactions of DRF 4367. The formation of M1 was extensively inhibited, by quinidine (2 μM, 98.5%) and ticlopidine (10 μM, 93.6%), suggesting involvement of both CYP2D6 and CYP2C19 (in man) in the phase I metabolism of DRF 4367.

Metabolism by phase II enzymes

When DRF 6574 (demethylated product of DRF 4367) was used as substrate for glucuronidation (in mouse, rat, dog, monkey and human liver microsomes in presence

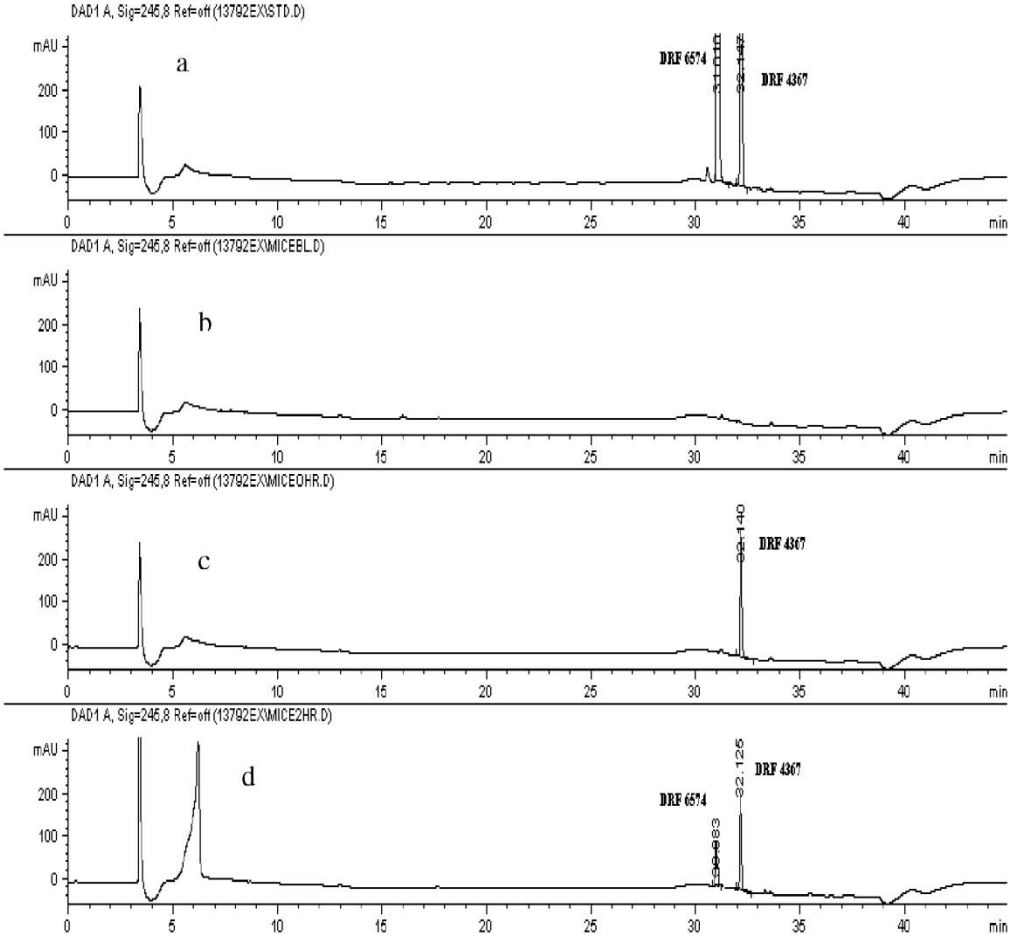

Figure 4. Representative chromatograms of mouse liver microsomal incubation studies: (a) injected standards; (b) mouse liver microsomes blank; (c) 0 min mouse liver microsomal incubation with DRF 4367 and 1 mM $NADP^+$; (d) 30 min mouse liver microsomal incubation with DRF 4367 and 1 mM $NADP^+$.

of UDPGA), one peak was detected by HPLC, namely M1-G, which disappeared after β-glucuronidase hydrolysis (data not shown). LC-MS analysis revealed a protonated molecular ion $(M + H)^+$ at *m/z* 590, 176 Da higher than M1, suggesting monoglucuronide formation (data not shown). Similarly, when DRF 6574 was used as the substrate for the sulfation reaction, one peak was detected by HPLC, namely M1-S, which disappeared after cincubation with arylsulfatase. LC-MS analysis revealed a protonated molecular ion $(M+H)^+$ at *m/z* 494, 80 Da higher than M1, suggesting monosulfoconjugation (data not shown). Further, when DRF 6574 was submitted to the simultaneous double reaction of conjugation (sulfation and glucuronidation), the HPLC profile was identical to the elution profile of the glucuronidation medium (data not shown). Therefore, DRF 6574 showed a propensity to form glucuronide conjugate in spite of the availability for a sulfation reaction. DRF 4367 failed to react, when it was used as a substrate for glucuronidation of sulfation under similar conditions in liver microsomes of various animal species tested.

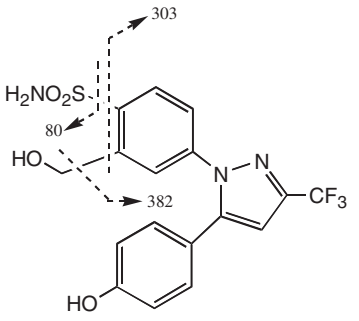

Product ions of *m/z* 412 (**M1 or DRF 6574**)

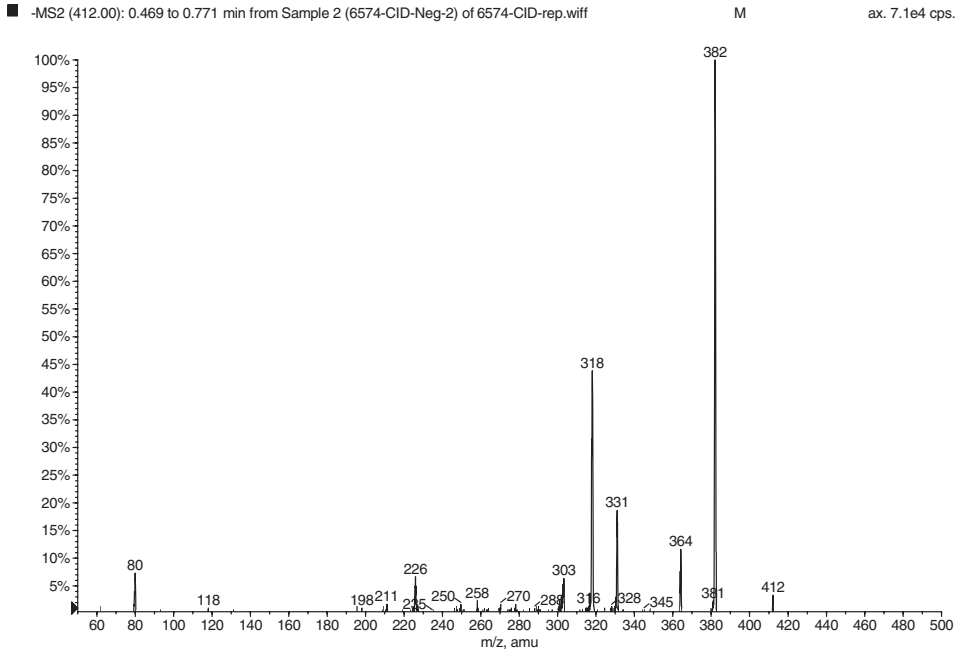

Figure 5. Representative CID spectrum of M1 or DRF 6574.

Incubation of bile with β-glucuronidase and arylsulfatase

HPLC analysis of bile collected from mice dosed with DRF 4367 showed two major peaks (peak 1, R.T: 26.9 min and peak 4, R.T: 34.9 min) and two minor peaks (peak 2, R.T: 31.2 min and peak 3, R.T: 32.3 min) (Figure 7). Peak 2 and peak 3 were tentatively assigned as M1 and DRF 4367, respectively, based on the retention times and UV spectrum of synthetic standards. When aliquots of bile sample were incubated with β-glucuronidase, peak 1 completely disappeared from the chromatogram (with no change in the area of peak 4), and a corresponding increase in peak 2 area was observed, suggesting it was an *O*-glucuronide conjugate of M1 (M1-G). Further, when the same bile sample was incubated with arylsulfatase, a complete decrease in area of peak 4 was observed with a corresponding increase in M1 area, suggesting peak 4 to be an *O*-sulfate conjugate of M1 (M1-S). Peak 1 was found to be unchanged after arylsulfatase incubation.

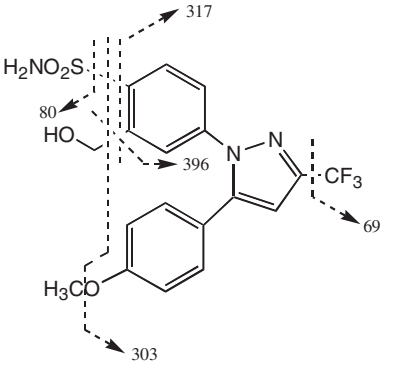

Product ions of *m/z* 426 (**DRF 4367**)

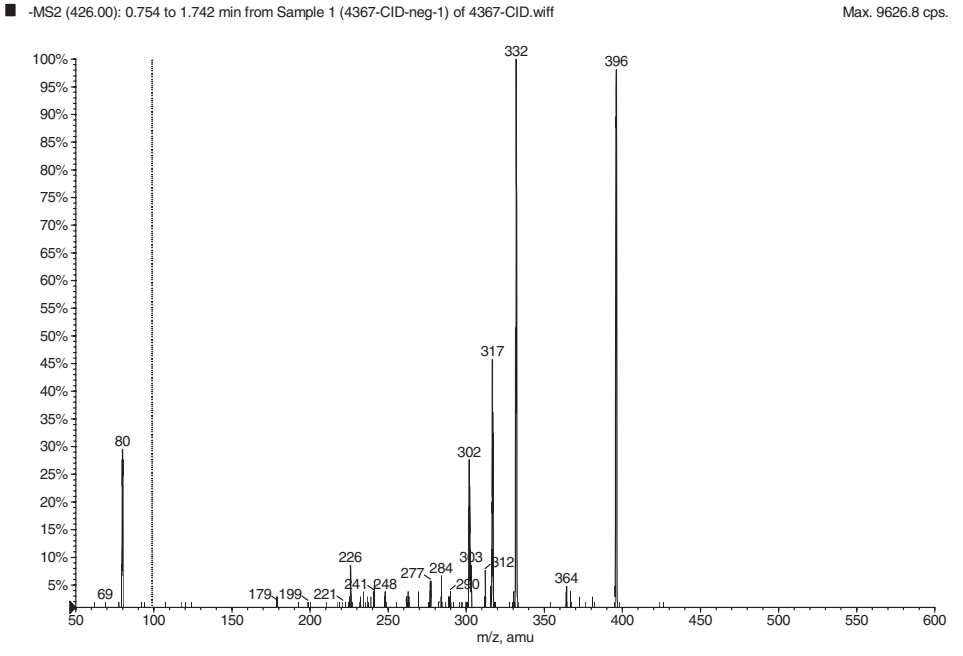

Figure 6. Representative CID spectrum of DRF 4367.

LC-MS/MS identification of metabolites in bile

The tentative identities assigned above to the parent and metabolites corresponding to peaks 1–4 in Figure 7 were confirmed by LC-MS/MS analysis in negative ion mode. As peaks 2 and 3 have a given similar CID spectrum (Figures 5 and 6) to that of authentic synthetic standards, i.e. DRF 6574 and DRF 4367, they were confirmed as M1 and DRF 4367, respectively. Figure 8 shows a representative CID spectrum of peak 1 or M1-G. This metabolite exhibited a deprotonated molecular ion at *m/z* 588. The CID spectrum of *m/z* 588 generated a series of product ions at *m/z* 570, 514, 412, 382, 331, 175 and 113.

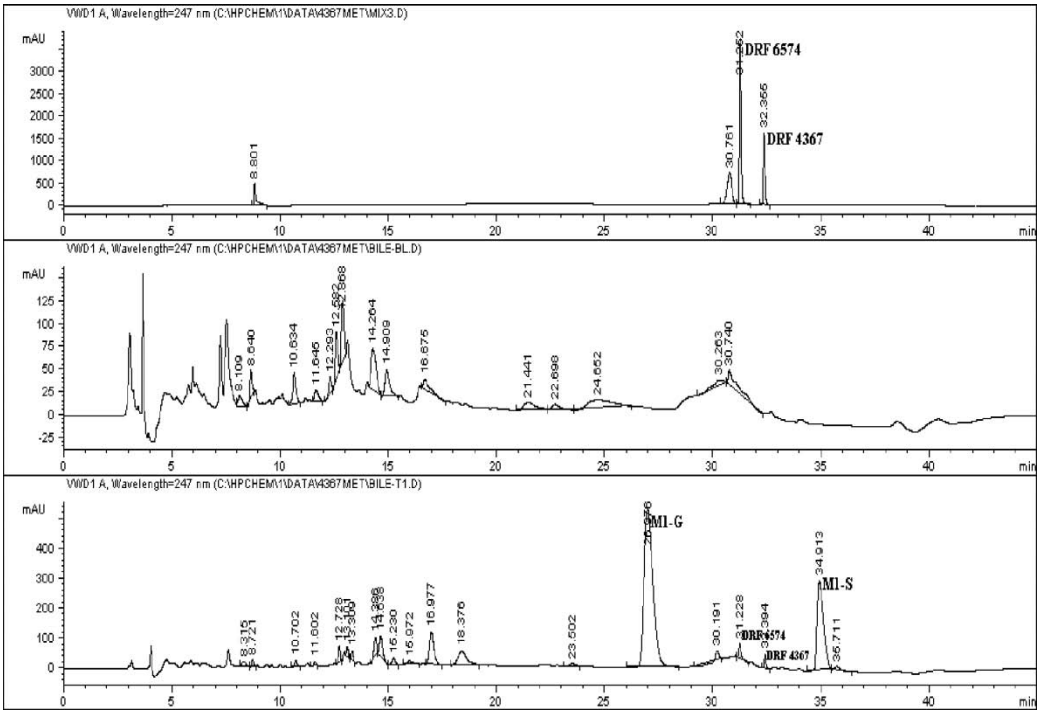

Figure 7. Representative HPLC chromatograms of mouse bile after *intravenous* administration of DRF 4367. Top panel: injected standards; middle panel: control bile; bottom panel: mouse bile collected after *intravenous* administration.

The product ion at *m/z* 412 (corresponding to *m/z* of M1) was generated through neutral loss of 176 Da, a characteristic cleavage for glucuronide conjugates. The product ions at *m/z* 382 and 331 were similar to those in the CID spectrum of M1. The product ion at *m/z* 570 is due to loss of 18 (H_2O) from the M1-G. The sequential loss of 74 (glyoxylic acid or CHOCOOH) and 102 (CHOHCHOHCCHOH) from *m/z* 588 generated ions at *m/z* 514 and 412, respectively. The product ions at *m/z* 175 and 113 were generated by sequential loss of 18 (H_2O) and 62 ($HOCH_2CH_2OH$) from glucuronic acid and confirmed the existence of glucuronic acid. Based on these data, peak 1 or M1-G was identified as the *O*-glucuronide of M1. The CID spectrum of peak 4 or M1-S is shown in Figure 9. This peak has a deprotonated molecular ion at *m/z* 492. The CID spectrum of *m/z* 492 generated a series of product ions at *m/z* 412, 382, 331, 318 and 80. The product ion at *m/z* 412 (corresponding to *m/z* of M1) was generated through neutral loss of 80 Da, a characteristic cleavage for sulfate conjugates. The product ions at *m/z* 382, 331 and 318 were similar to those in the CID spectrum of M1. The product ion at *m/z* 80 corresponds to either the SO_3 or SO_2NH_2 groups. Based on these data, peak 4 or M1-S was identified as *O*-sulfate conjugate of M1.

Profiling in urine, feces and plasma

HPLC and LC-MS analysis of urine collected from mice following oral and IV administration revealed the presence of M1-G and M1-S in trace quantities, but no DRF 4367

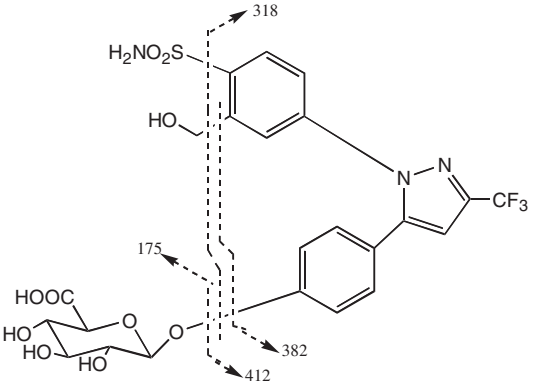

Product ions of *m/z* 588 (**M1-G**)

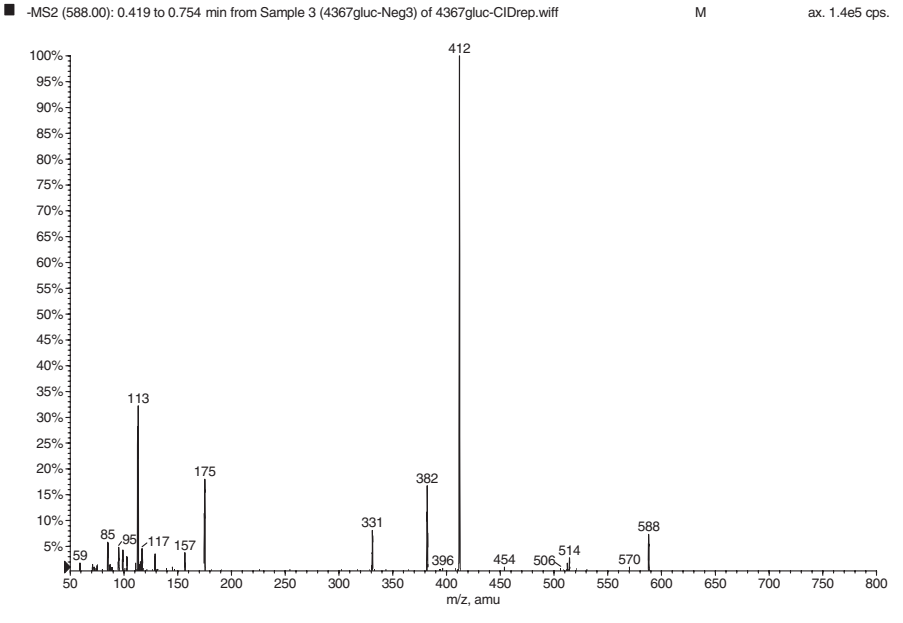

Figure 8. Representative CID spectrum of M1-G.

and M1 were detected. On the contrary, feces showed the presence of DRF 4367 and M1. M1-G and M1-S were not detected in feces. Plasma has predominant concentrations of DRF 4367, and the concentrations of M1 were much lower than those of DRF 4367. Using all of the above *in vitro* and *in vivo* information, a proposed scheme for the metabolism of DRF 4367 in mice is presented in Figure 10.

Discussion

Owing to the availability of the plethora of pharmacokinetic and metabolism information on marketed coxibs such as celecoxib, rofecoxib, valdecoxib, etoricoxib, lumiracoxib (Figure 1) (Halpin et al. 2000, 2002; Paulson et al. 2000a, b; Chauret et al. 2001; Yuan et al. 2002; Rodrigues et al. 2003; Zhang et al. 2003; Mangold et al. 2004) and coxibs under

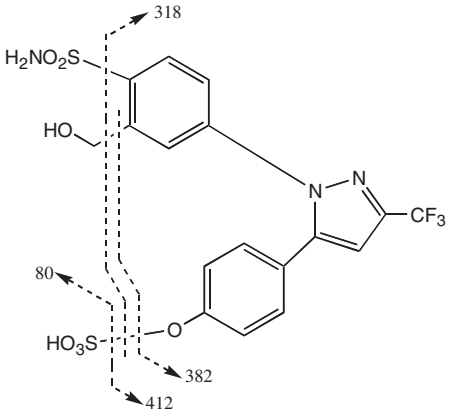

Product ions of *m/z* 492 (**M1-S**)

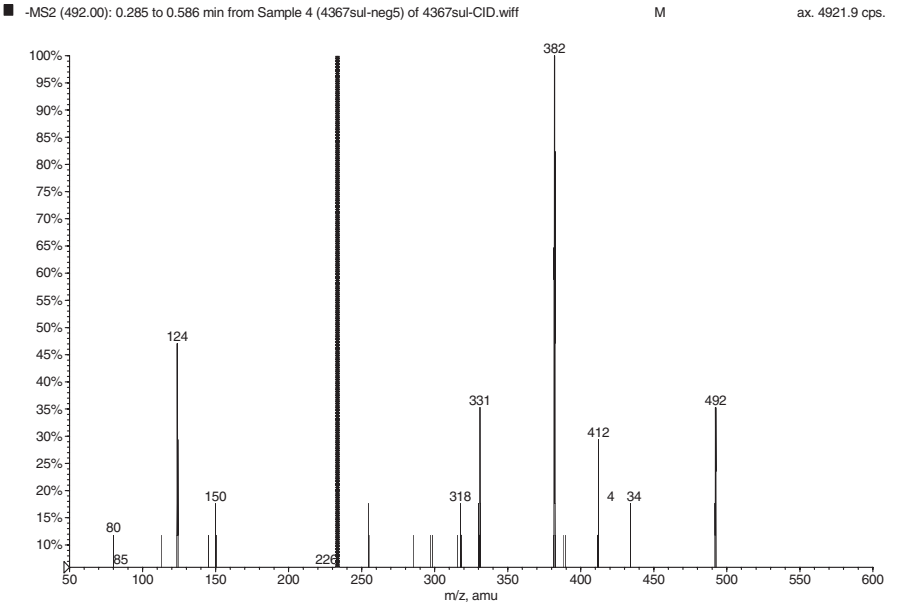

Figure 9. Representative CID spectrum of M1-S.

development such as DRF 4367 and DRF 4848 (Ramesh et al. 2003; Singh et al. 2004), we were interested to profile further the pharmacokinetic disposition and understand aspects of metabolism of DRF 4367, a novel diaryl coxib compound in pre-clinical species.

Previously, in a single dose oral pharmacokinetic study in male Wistar rats (doses: 2–10 mg kg^{-1}), both C_{max} and $AUC_{(0-\infty)}$ values of DRF 4367 increased in a linear fashion as the administered doses increased. However, when the oral doses of DRF 4367 were greater than 30 mg kg^{-1}, the increments in both C_{max} and $AUC_{(0-\infty)}$ ceased to be linearly related to dose but were found to be less than proportional (Ramesh et al. 2003). This phenomenon has been observed with other coxibs owing to their poor solubility. In the present study, the oral bioavailability of DRF 4367 was found to be approximately 44% at 10 mg kg^{-1}. The issue of poor bioavailability has been overcome by preparing a solubilized

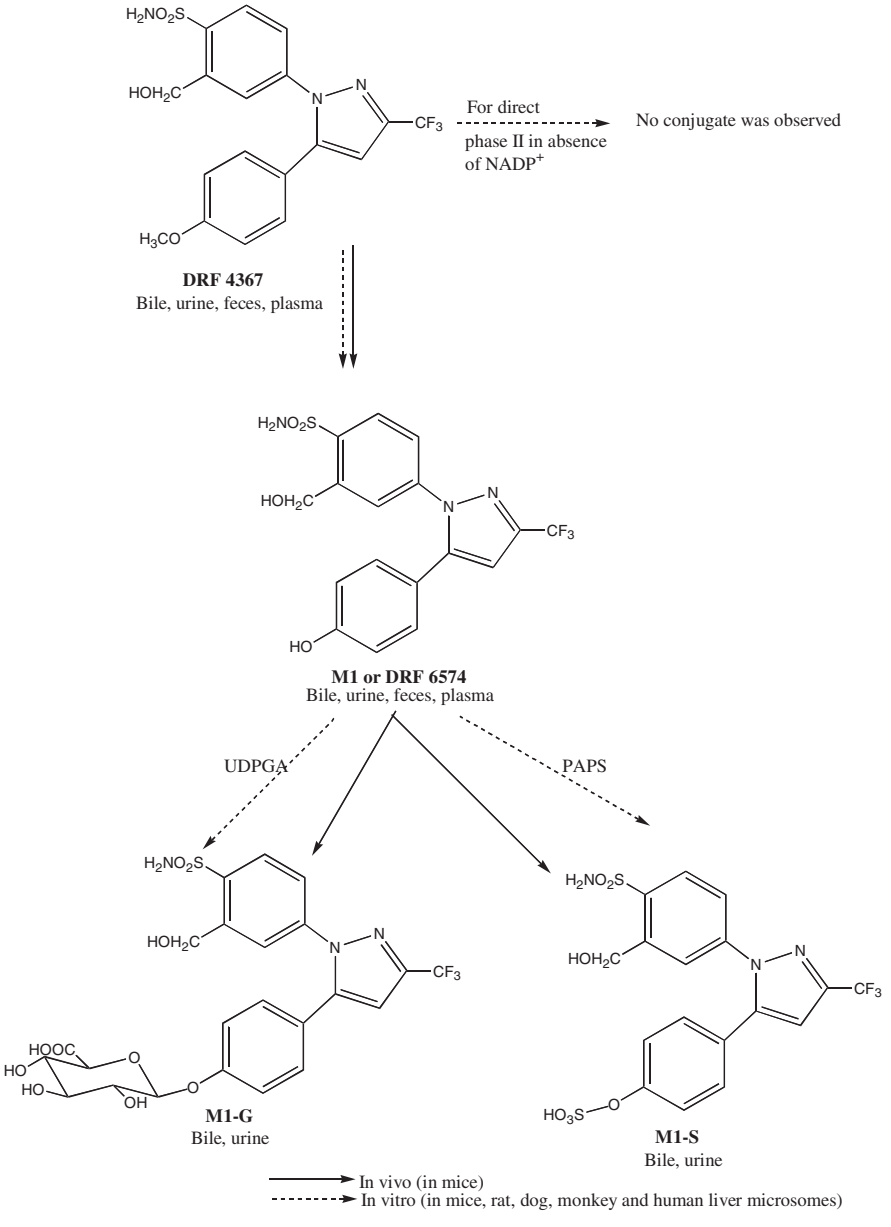

Figure 10. Proposed metabolic pathway for DRF 4367.

formulation of coxib and/or using a prodrug approach to liberate the needed parent molecule in the systemic circulation (Mamidi et al. 2002). Therefore, it is possible that one of the above approaches can be effectively used to enhance the oral bioavailability of DRF 4367 especially at higher doses.

Since coxibs are known to have problems related to absorption at higher doses resulting in decreased bioavailability as the dose is increased, it is very important to understand the metabolism aspects at doses that promote maximum absorption and optimal bioavailability.

As a first step towards understanding the metabolism of DRF 4367, we have performed a series of *in vitro* metabolism studies in liver microsomes of various species. In this regard, *in vitro* and *in vivo* metabolic investigations of marketed coxibs such as celecoxib, rofecoxib, valdecoxib, etoricoxib and lumaricoxib have revealed qualitatively the formation of oxidative phase I metabolites and the phase II metabolites comprising the conjugates of glucuronic acid (Paulson et al. 2000a, b; Halpin et al. 2000, 2002; Chauret et al. 2001; Yuan et al. 2002; Rodrigues et al. 2003; Zhang et al. 2003; Mangold et al. 2004) and sulfate (Halpin et al. 2000). However, a much closer look at the metabolic pathways and the metabolites formed (both phase I and phase II) suggests a degree of subtle changes in the metabolic patterns of coxibs owing to certain unique structural features of the coxib substrates.

The novel COX-2 inhibitor, DRF 4367, has been shown to be metabolized primarily by demethylation of the benzyl methoxy group to form M1. M1 was found to undergo glucuronidation and sulfation (M1-G and M1-S), and the latter two metabolites were excreted as major metabolites along with the parent compound and M1 (as minor ones) in bile. Both the conjugates were present in urine at trace levels and absent in feces and plasma. DRF 4367 and M1 were found in feces and plasma but were not detected in urine. Regardless of the species of liver microsomes tested, the *in vitro* metabolic pathway of DRF 4367 involved a demethylation of the benzyl methoxy group to a hydroxy metabolite (M1). The formation of M1 was mediated by human CYP2D6 and CYP2C19. M1 undergoes phase II metabolism (in the absence of $NADP^+$) to form the either glucuronide or sulfate conjugate in the presence of UDPGA or PAPS, respectively, in mouse and human liver microsomes. On the contrary, the parent molecule (DRF 4367) when subjected to direct phase II metabolism (in the absence of $NADP^+$) did not form any conjugate. In order to confirm the findings of the ease of M1 phase II conjugation, the hydroxy metabolite (M1) was synthesized in our laboratories. This newly synthesized molecule was found to readily undergo phase II metabolism. The synthesis of the primary metabolite and the ability to form the phase II conjugate demonstrated that phase II metabolism occurred at the free hydroxyl group but not on the hydroxy methyl group. Although the inability of the hydroxyl methyl group to participate in the phase II conjugation was somewhat of a surprise to us, we postulate a probable reason for this observation. Because the hydroxyl methyl group is located adjacent to a SO_2NH_2 group, there is a likely possibility of formation of stable intra-molecular hydrogen bonding between these groups. When we subjected the structure of DRF 4367 to computational molecular modeling, intra-molecular hydrogen bonding was confirmed (Singh et al. 2004). The formation of intra-molecular hydrogen bond prevents the hydroxyl methyl group to undergo both phase I and/or direct phase II metabolism. Recently published metabolism data on a novel COX-2 inhibitor, indomethacin phenethylamide, revealed the formation of intra-molecular hydrogen bonding, which offered enhanced stability for one of the metabolites, namely, 1′-hydroxy indomethacin phenethylamide (Remmel et al. 2004). As a result of this phenomenon, although structurally it represented a carbinolamide, further phase II conjugation of this metabolite was not observed. It was postulated that the 1′-hydroxy group formed a stable six-membered ring confirmation via an intra-molecular hydrogen bond with the adjacent carbonyl substituent. On the contrary, the 2′-hydroxy metabolite of indomethacin phenethylamide underwent phase II conjugation with glucuronic acid (Remmel et al. 2004). The above data offer further justification for our proposed hypothesis of the intra-molecular hydrogen bond that protects the site from undergoing any phase I or phase II metabolism. Contrary to our findings on DRF 4367, the case study of celecoxib reveals that the benzyl methyl group undergoes oxidation to give a hydroxy metabolite, which further undergoes oxidation to the carboxylic acid group.

Both the hydroxyl and carboxylic acid metabolites have been demonstrated to form glucuronide conjugates (Paulson et al. 2000a, b). In a similar manner, etoricoxib undergoes an identical type of phase I metabolism and forms both hydroxyl and carboxylic acid metabolites, in addition to the formation of a *N*-oxide metabolite. Unlike celecoxib, etoricoxib forms predominantly the hydroxyl methyl glucuronide as compared with the carboxylic acid glucuronide (Chauret et al. 2001). Another COX-2 inhibitor, valdecoxib undergoes extensive metabolism by hydroxylation of a methyl group or *N*-hydroxylation at the sulfonamide or on the free phenyl ring along with several minor phase I metabolites. In addition to the latter metabolites, formation of *O*-glucuronides (of hydroxylated metabolites) and N-glucuronides (direct on the sulfonamide group or *N*-hydroxylated) were also reported (Yuan et al. 2002). As the sulfonamide group is free in the case of valdecoxib (Figure 1) it participates in both phase I and direct phase II reactions. Our hypothesis for the formation of intra-molecular hydrogen bonding holds further credence when a careful evaluation of structures of the celecoxib and etoricoxib (Figure 1) is performed. Both celecoxib and etoricoxib show a distinct separation of the SO_2NH_2 group and methyl group. Since the possibility of intra-molecular hydrogen bonding is not possible for both celecoxib and etoricoxib, the methyl group readily undergoes oxidative metabolism and subsequently phase II metabolism.

The presence of active circulating metabolites can influence the doses to be administered as well as the dosing regimen. Having confirmed that the primary metabolite identified *in vitro* is also found *in vivo*, the synthesized metabolite, DRF 6574, was tested for inhibition of COX-1 and COX-2 in the standard human whole blood assays. We confirmed that the metabolite was not active (data not shown), and therefore, it is not anticipated to contribute to the benefits of COX-2 inhibition and/or any of the potential side effects associated with COX-1 inhibition.

References

Chauret N, Yergey JA, Brideau C, Friesen RW, Mancini J, Riendeau D, Silva J, Styhler A, Trimble AS, Nicoll-Griffth DA. 2001. In vitro metabolism considerations, including activity testing of metabolites, in the discovery and selection of COX-2 inhibitor etoricoxib (MK-0663). Bioorganic Medicinal Chemistry Letters 11:1059–1062.

DeWitt LD. 1999. COX-2 selective inhibitors: The new super aspirins. Molecular Pharmacology 4:625–631.

Gibaldi M, Perrier D. 1982. Pharmacokinetics. 2nd ed. New York: Dekker.

Gierse JK, Hauser SD, Creely DP, Koboldt C, Rangwala SH, Isakson PC, Seibert K. 1995. Expression and selective inhibition of the constitutive and inducible forms of human cyclo-oxygenase. Biochemical Journal 305:479–484.

Gradolatto A, Canivenc-Lavier MC, Basly JP, Siess MH, Teyssier C. 2004. Metabolism of apigenin by rat liver phase I and phase II enzymes and by isolated perfused rat liver. Drug Metabolism and Disposition 32:58–65.

Graul A, Martel AM, Castaner RM. 1997. Celecoxib: Antiinflammatory cyclooxygenase inhibitor. Drugs of Future 22:711–714.

Halpin RH, Geer LA, Zhang KE, Marks TM, Dean DC, Jones AN, Melillo D, Doss G, Vyas KP. 2000. The absorption, distribution, metabolism and excretion of rofecoxib, a potent and selective cyclooxygenase-2 inhibitor, in rats and dogs. Drug Metabolism and Disposition 28:1244–1254.

Halpin RA, Porras AG, Geer LA, Davis MR, Cui D, Doss GA, Woolf E, Musson D, Matthews C, Mazenko R, Schwartz JI, Lasseter KC, Vyas KP, Baillie TA. 2002. The disposition and metabolism of rofecoxib, a potent and selective cyclooxygenase-2 inhibitor, in human subjects. Drug Metabolism and Disposition 30:684–693.

Rao MNVS, Biju B, Ansar AK, Mujeeb S, Ramesh M, Srinivas NR. 2003. Open access generic method for continuous determination of major human CYP 450 substrates/metabolites and its application in drug metabolism studies. Xenobiotica 12:1233–1245.

Mamidi RNVS, Mullangi R, Kota J, Bhamidipati R, Khan AA, Katneni K, Datla S, Singh SK, Rao YK, Seshagiri Rao C, Srinivas NR, Rajagopalan R. 2002. Pharmacological and pharmacokinetic evaluation of celecoxib prodrugs in rats. Biopharmaceutics and Drug Disposition 23:273–282.

Mangold JB, Gu H, Rodriguez LC, Bonner J, Dickson J, Rordorf C. 2004. Pharmacokinetics and metabolism of lumiracoxib in healthy male subjects. Drug Metabolism and Disposition 32:566–571.

Paulson SK, Hribar JD, Liu NW, Hajdu E, Bible RH, Piergies A, Karim A. 2000a. Metabolism and excretion of [^{14}C] celecoxib in healthy male volunteers. Drug Metabolism and Disposition 28:308–314.

Paulson SK, Zhang JY, Breau AP, Hribar JD, Liu NW, Jessen SM, Law YM, Cogburn JN, Gresk CJ, Markos CS, Maziasz TJ, Schoenhard GL, Burton EG. 2000b. Pharmacokinetics, tissue distribution, metabolism, and excretion of celecoxib in rats. Drug Metabolism and Disposition 28:514–521.

Ramesh M, Mamidi RNVS, Jaganath K, Singh SK, Rao YK, Seshagiri Rao C, Rajagopalan R, Srinivas NR. 2003. Oral bioavailability and pharmacokinetics of DRF 4367, a new cox-2 inhibitor in rats. European Journal of Drug Metabolism and Pharmacokinetics 28:137–141.

Ramesh M, Reddy RK, Ravikanth B, Mamidi RNVS, Srinivas NR. 2004. HPLC method for determination of DRF 4367 in rat plasma: Validation and its application to pharmacokinetics in Wistar rats. Biomedical Chromatography 18:576–580.

Remmel RP, Crews BC, Kozak KR, Amit AS, Marnett LJ. 2004. Studies on the metabolism of the novel, selective cyclooxygenase-2 inhibitor indomethacin phenethylamide in rat, mouse, and human liver microsomes: Identification of active metabolites. Drug Metabolism and Disposition 32:113–122.

Riendeau D, Charleson S, Cromlish W, Mancini JA, Wong E, Guay J. 1997. Comparison of the cyclooxygenase-1 inhibitory properties of non-steroidal anti-inflammatory drug (NSAIDs) and selective COX-2 inhibitors, using sensitive microsomal and platelet assays. Canadian Journal of Physiology and Pharmacology 57:465–480.

Rodrigues DA, Halpin RA, Geer LA, Cui D, Woolf EJ, Matthew CZ, Gottesdiener KM, Larson PJ, Lasseter KC, Agrawal GB. 2003. Absorption, metabolism, and excretion of etoricoxib, a potent and selective cyclooxygenase-2 inhibitor, in healthy male volunteers. Drug Metabolism and Disposition 31:224–232.

Singh SK, Ganapati Reddy P, Srinivasa Rao K, Lohray BB, Seshagiri Rao C, Misra P, Rajjak SA, Rao YK, Venkateswarlu A. 2004. Polar substitutions in the benzenesulfonamide ring of celecoxib afford a potent 1,5-diarylpyrazole class of COX-2 inhibitors. Bioorganic Medicinal Chemistry Letters 14:499–504.

Smith WL, DeWitt DL. 1996. Prostaglandin endoperoxide H synthases-1 and 2. Advance Immunology 62:67–215.

Teyssier C, Siess MH. 2000. Metabolism of dipropyl disulfide by rat liver phase I and phase II enzymes and by isolated perfused rat liver. Drug Metabolism and Disposition 28:648–654.

Vane JR, Bakhle YS, Botting RM. 1998. Cyclooxygenase 1 and 2. Annual Reviews in Pharmacology and Toxicology 47:1151–1156.

Yuan JJ, Yang DC, Zhang JY, Bible R, Karim A, Findlay JWA. 2002. Disposition of a specific cyclooxygenase-2 inhibitor, valdecoxib, in human. Drug Metabolism and Disposition 30:1013–1021.

Zhang JY, Yuan JJ, Wang YF, Bible RH, Breau AP. 2003. Pharmacokinetics and metabolism of a COX-2 inhibitor, valdecoxib, in mice. Drug Metabolism and Disposition 31:491–501.